

Accepted Manuscript

Comparative study of core-shell nanostructures based on amino-functionalized $\text{Fe}_3\text{O}_4@\text{SiO}_2$ and $\text{CoFe}_2\text{O}_4@\text{SiO}_2$ nanocomposites

P. Arévalo-Cid, J. Isasi, F. Martín-Hernández



PII: S0925-8388(18)32367-3

DOI: [10.1016/j.jallcom.2018.06.246](https://doi.org/10.1016/j.jallcom.2018.06.246)

Reference: JALCOM 46582

To appear in: *Journal of Alloys and Compounds*

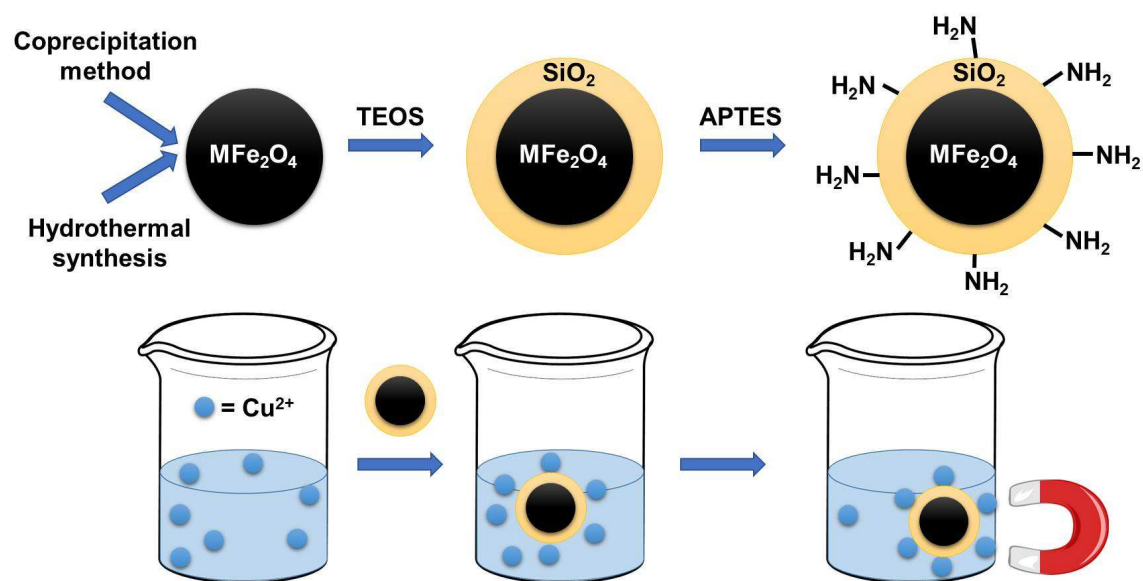
Received Date: 21 March 2018

Revised Date: 23 May 2018

Accepted Date: 20 June 2018

Please cite this article as: P. Arévalo-Cid, J. Isasi, F. Martín-Hernández, Comparative study of core-shell nanostructures based on amino-functionalized $\text{Fe}_3\text{O}_4@\text{SiO}_2$ and $\text{CoFe}_2\text{O}_4@\text{SiO}_2$ nanocomposites, *Journal of Alloys and Compounds* (2018), doi: 10.1016/j.jallcom.2018.06.246.

This is a PDF file of an unedited manuscript that has been accepted for publication. As a service to our customers we are providing this early version of the manuscript. The manuscript will undergo copyediting, typesetting, and review of the resulting proof before it is published in its final form. Please note that during the production process errors may be discovered which could affect the content, and all legal disclaimers that apply to the journal pertain.



Comparative study of core-shell nanostructures based on amino-functionalized $\text{Fe}_3\text{O}_4@\text{SiO}_2$ and $\text{CoFe}_2\text{O}_4@\text{SiO}_2$ nanocomposites.

P. Arévalo-Cid¹, J. Isasi^{1*}, F. Martín-Hernández^{2,3,4}.

¹*Departamento de Química Inorgánica I, Facultad de Ciencias Químicas, Universidad Complutense de Madrid, Ciudad Universitaria s/n, 28040 Madrid, Spain.*

²*Departamento de FTAA I, Facultad de Ciencias Físicas, Universidad Complutense de Madrid, Ciudad Universitaria s/n, 28040 Madrid, Spain.*

³*Instituto de Geociencias (UCM, CSIC), 28040 Madrid, Spain.*

⁴*Instituto de Magnetismo Aplicado (UCM), 28230 Las Rozas, Spain.*

Abstract

$\text{Fe}_3\text{O}_4@\text{SiO}_2$ and $\text{CoFe}_2\text{O}_4@\text{SiO}_2$ and their corresponding amino-functionalized nanocomposites were successfully synthesized by a process of two steps including the preparation by coprecipitation or hydrothermal synthesis of the corresponding magnetic cores, the coating of its surface with a silica coating followed by its subsequent functionalization with 3-aminopropyltriethoxysilane (APTES). All magnetic samples were characterized by XRD using FULPROFF program, FTIR analysis, TEM and M-H hysteresis loops. The results showed diffraction maxima indexed in a cubic symmetry of S. G. Fd-3m with Z = 8 compatible with an inverse spinel-type structure. FTIR spectra of all samples show the characteristic bands of the magnetic cores and others bands corresponding to the asymmetric vibration of O-Si-O and Si-O-Si bonds of silica. The TEM images confirm that all the nanoparticles are coated, finding the largest thickness of the coating in the Fe_3O_4 sample prepared hydrothermally, which are the smaller ones. An expected reduction of the saturation magnetization of the magnetic cores is achieved

with the coating and functionalization, although the behavior of the Fe_3O_4 -samples remains practically superparamagnetic while the corresponding ones of cobalt are still ferrimagnetic. Fe_3O_4 nanocomposites respond to more quickly in the presence of an external magnetic field, something important against the removal of contaminating species in aqueous media. UV-Vis spectroscopy studies confirm the adsorption capacity of Cu^{2+} in aqueous solutions of the prepared nanocomposites, having found that a small thickness of the coating leads a greater adsorption, so that the best adsorption is found for CP- Fe_3O_4 @ SiO_2 -APTES nanocomposite.

Keywords: Nanocomposites, Magnetic properties, Ferrites, Cations Removal

* Corresponding author

e-mail: isasi@.ucm.es

Phone: +34 913945215

Fax: +34 913944352

1. Introduction

Water pollution caused by heavy metal cations can cause a variety of negative effects on human health, even if those metal cations are in low concentrations [1-4]. They get into water system via several manufacturing processes such as refining, fertilizer, and pesticides and suppose a severe risk to the aquatic environment, where the low biodegradability and bioaccumulation tendency of these metals could give rise to intake and accumulate in the fish body to end up entering food chain [5-7]. Based on these potential risks, there is currently a continuously increasing worldwide concern for the development of wastewater treatment technologies, including the testing of new synthesis methods, which allow the obtaining of suitable nanostructures to solve this type of problems [8-10]. For this reason, we are researching in obtaining of suitable

nanostructures that allow acting in the preconcentrating and subsequent removal of heavy metals cations.

Different methods of removing heavy metal cations from wastewater have been tested over the years, including: membrane separation [11, 12], coagulation–flocculation [13, 14], chemical precipitation [15, 16], flotation [17], reverse osmosis [18, 19], ion exchange [20, 21], solvent extraction [22, 23], adsorption [24], etc. Some of these methods have their own disadvantages such as low efficiency, sensitive working to environments and production of toxic slurry. Among these, adsorption is an attractive method owing to its simplicity and high efficiency [25]. To date, different materials with adsorbent capacity have been synthesized [26-29], although not many have proved useful for the removal of heavy metals ions. For this reason, obtaining of sorbents with high adsorption capacity, easy separation and recyclability is a challenge today and its synthesis and design are of great scientific and technological importance.

Nanotechnology can provide opportunities to meet the challenge of to be able to isolate materials with adequate adsorption capacity. Magnetic adsorbents materials with core-shell nanostructure have attracted much interest owing their synergistic effect between its multiple components and the resulting new properties [30, 31]. In these nanostructures, magnetic nanoparticles incorporate a surface coating that reduces its agglomeration and prevents its subsequent oxidation. The magnetic core can facilitate a rapid separation and the coating may exhibit functional groups having a high affinity for toxic metals and increasing their adsorption potential [34, 35].

Different researches have been carried out on the design of core-shell magnetic nanocomposites. Among these core-shell nanostructures, the use of Fe_3O_4 nanoparticles as core has been widely studied owing to their unique magnetic characteristics. Abd Ali

et al. [36] described a novel chrysin-functionalized Fe_3O_4 core for the removal of Cu^{2+} from aqueous solutions and found an adsorption capacity of 114 mg. g^{-1} , value comparable to that determined by Asthana et al. (120 mg. g^{-1}) in a Fe_3O_4 @glycine composite [37]. Bao et al. [38] also published the synthesis and study of a mercaptoamine-functionalized silica-coated magnetite for the removal of toxic metals such as Pb^{2+} with a maximum adsorption capacity of 292 mg. g^{-1} .

Many studies describe the use of nanocomposites of magnetite cores as adsorbent materials, however, it should be noted that the low chemical stability of Fe_3O_4 nanoparticles, even when coated, could avoid rapid magnetic separation of toxic pollutants. In relation to Fe_3O_4 oxide, CoFe_2O_4 nanoparticles are much more chemically stable, easy to prepare and exhibiting a moderate saturation to achieve a rapid separation [39]. Different studies describe the preparation of CoFe_2O_4 @ SiO_2 nanocomposites and reflect the isolation of materials with large and agglomerates particles, which reduces their adsorption capacity [40-42]. As in the case of Fe_3O_4 @ SiO_2 studied samples, to improve its performance the surfaces can also be modified by different functional chemical groups. 3-aminopropyltriethoxysilane (APTES) is a commonly used coupling agent. Amino groups can react with heavy metals ions allowing their removal of the aqueous solutions. This paper describes, for the first time, a comparative study of amino-functionalized Fe_3O_4 @ SiO_2 and CoFe_2O_4 @ SiO_2 samples whose magnetic cores were prepared by two different synthesis methods. Their effect on powder morphology and magnetic properties is analyzed. Functionalization of silica nanocomposite surfaces and adsorption capacity of Cu^{2+} cations in aqueous solution of synthesized nanocomposites have also been evaluated by UV-Vis spectroscopy.

2. Experimental

2.1. Synthesis of Fe_3O_4 and $CoFe_2O_4$ samples by coprecipitation.

Fe_3O_4 and $CoFe_2O_4$ nanopowders were prepared by coprecipitation of the respective starting materials, $FeCl_3 \cdot 6 H_2O$ (Strem Chemicals, 97%) and $FeCl_2 \cdot 6 H_2O$ (Sigma Aldrich, 99%) or $CoCl_2 \cdot 6 H_2O$ (Panreac, PA). Stoichiometric quantities of $FeCl_3 \cdot 6 H_2O$ (1.083 g, 4 mmol) and $FeCl_2 \cdot 6 H_2O$ (0.397 g, 2 mmol) or $CoCl_2 \cdot 6 H_2O$ (0.476 g, 2 mmol), in a 2:1 ratio, were dissolved in 150 ml of distilled water into two glass reactors under both Ar atmosphere and mechanical stirring. After the addition of 20 ml of NH_3 at 25%, a colour change was appreciated from yellow to black/dark brown in the two solutions, due to the precipitation of metal hydroxides [43]. Final mixtures were heated at 75 °C and stirred for 30 min. Subsequently, oleic acid (OA) was added to the different solutions and dispersion is favored [43, 44]. These reactions were maintained for 60 min. The products were obtained as precipitates that were collected by magnetic separation and washed several times with a mixture of water/acetone. Nanopowders resulting were dried in stove at 50 °C. For the obtaining of $CoFe_2O_4$ sample it was also necessary to carry out an additional thermal treatment at 300 °C for 2 h. The synthesized samples are named as CP- Fe_3O_4 and CP- $CoFe_2O_4$.

2.2. Preparation of Fe_3O_4 and $CoFe_2O_4$ samples by hydrothermal synthesis.

Fe_3O_4 and $CoFe_2O_4$ samples were prepared from the respective metal precursor, $Fe(NO_3)_3 \cdot 9 H_2O$ (Aldrich, 98+%) (2 mmol, 0.808 g), $Co(NO_3)_2 \cdot 6 H_2O$ (Panreac, PA) (1 mmol 0.291 g) and iron (II) sulphate $Fe(SO_4) \cdot 7 H_2O$ (Sigma Aldrich, >98%) (1 mmol, 0.278 g). Stoichiometric quantities were dissolved in two beakers, with addition of distilled water and, later, they were homogenized by mechanical stirring under Ar atmosphere. 5 ml of KOH 2M solution was added as mineralizing agent to these beakers. The resulting solutions were transferred to two teflon-lined stainless-steel

autoclaves and were heated during 3 hours at 120° and at 180°C for obtaining of Fe₃O₄ and CoFe₂O₄ samples, respectively. Finalized the thermal treatment, corresponding nanopowders were isolated by magnetic decantation. Synthesized samples are named as HT-Fe₃O₄ and HT-CoFe₂O₄.

2.3. Synthesis Fe₃O₄@SiO₂ and CoFe₂O₄@SiO₂ nanocomposites.

Synthesis of these nanocomposites was carried out using Stöber method [45]. 0.1 g of the corresponding magnetic samples were placed in an Erlenmeyer flask assisted by an ultrasonic bath for 10 min and were dispersed in 50 mL of distilled water, 150 mL of ethanol and 10 mL of ammonia at 32%. Then, 2 mL of tetraethoxysilane (TEOS), Si(OC₂H₅)₄, (Merck, synthesis grade) was added slowly under mechanical stirring and these reactions were maintained during 3h. The resulting white powders were separated by magnetic decantation and then washed with a mixture of water and ethanol. Synthesized samples are named as CP-Fe₃O₄@SiO₂ and HT-Fe₃O₄@SiO₂, CP-CoFe₂O₄@SiO₂ and HT-CoFe₂O₄@SiO₂.

2.4. Synthesis amino-functionalized Fe₃O₄@SiO₂ and CoFe₂O₄@SiO₂ nanocomposites.

These preparations were carried out starting from 0.1 g of the silica-magnetic samples suspended in 50 ml of isopropanol for 10 minutes. These suspensions were poured into round bottom flasks coupled to a refrigerant to which 0.6 mL of aminopropyltriethoxysilane Si(OC₂H₅)₃C₃H₆NH₂ (APTES) (Sigma Aldrich, 99%) was also added. All reactions were refluxed for 6 h and then allowed to cool. The powder samples were isolated by magnetic decantation and washed with isopropanol.

Synthesized samples are named as CP-Fe₃O₄@SiO₂-APTES and HT-Fe₃O₄@SiO₂-APTES, CP-CoFe₂O₄@SiO₂-APTES and HT-CoFe₂O₄@SiO₂-APTES.

2.5. Characterization

The structural characterization of the prepared samples was carried out by X-ray diffraction (XRD) employing an X'Pert-MPD Philips diffractometer with Cu K α radiation. A step scan of 0.04° (2 θ) in the range 10-120° and a counting time of 1s for each step were employed for data collection. The instrumental broadening of the diffraction peaks was considered and calibrated using the LaB6 standard NIST SRM 660b. Powder diffraction data were refined by the Rietveld method using the FullProf software [46, 47] and a Thompson-Cox-Hastings function to describe the peak shape. Fourier Transform Infrared (FTIR, IR-Prestige-21 Fourier Transform spectrometer) spectroscopy studies allow visualize the possible interaction between the magnetic samples, the silica covering and the amino functionalization. All FTIR spectra were measured on the 4000-400 cm⁻¹ region for samples dispersed in KBr pellets (at a 2:98 ratio). Transmission electron microscopy TEM was used to characterize the powders. A JEOL 2100F transmission electron microscope operating at 200 kV and equipped with a field emission electron gun providing a point resolution of 0.19 nm was employed. Samples were prepared by placing a drop of a dilute ethanol dispersion of nanoparticles onto a 300-mesh carbon coated copper grid prior to examination. The magnetization loops of the samples were measured at room temperature using a coercivities spectrometer developed by the University of Kazan (Coercivity Spectrometer J-meter) [48] and the field reached up to 5000 Oe. Adsorption studies of amino-funtionalized Fe₃O₄@SiO₂ and CoFe₂O₄@SiO₂ samples were monitored by UV-Vis spectroscopy, using a Jasco V-530 spectrometer, with a measure range 340-800 nm, using water as reference. In the tests performed, 30 mg of the respective nanocomposites were added to 30 mL of a 10⁻² M CuSO₄·5H₂O solution. An ultrasonic bath was used to disperse the powder and aliquots of the resulting suspension were taken over time. To increase the

intensity of the UV-Vis signal, the aliquots were treated with NH_3 at 32%, to form the complex $[\text{Cu}(\text{NH}_3)_4(\text{H}_2\text{O})_2]^{2+}$ with higher molar absorptivity. After the tests, the corresponding nanocomposites were separated by magnetic sedimentation, proceeding to the evaluation of its adsorbent capacity of Cu^{2+} cations.

3. Results and discussion

3.1. X-ray diffraction

Figure 1 shows the diffraction profiles of Fe_3O_4 and CoFe_2O_4 samples prepared by coprecipitation and hydrothermal synthesis. In all cases, the X-ray diffraction patterns show reflections which can be indexed to a tetragonal symmetry of S. G. $\text{Fd-}3\text{m}$ with $Z = 8$, compatible with an inverse spinel-type structure, characteristic of both Fe_3O_4 (JCPDS n° 82-1533) and CoFe_2O_4 oxides (JCPDS n° 22-1086).

More intense diffraction maxima are observed in the case of the samples prepared by hydrothermal synthesis. These results can be justified based on the pressure generated in the autoclave that contributes to the improvement of the crystallinity of these samples [49]. Table 1 shows the lattice parameters determined by the Chekcell program from XRD patterns.

Lattice parameters of the synthesized Fe_3O_4 and CoFe_2O_4 samples are in good agreement with those reported in the literature. The presence of Fe^{2+} ion in the Fe_3O_4 samples originates a higher somewhat higher cell parameter, justifiable by Shannon ionic radius of Fe^{2+} (0.78 Å) in relation to Co^{2+} (0.745 Å) [52]. An estimation of the average crystalline size of as-synthesized samples was made (see Table 1) using the Scherrer formula:

$$D_{\text{hkl}} = 0.89 \cdot \lambda / \beta \cdot \cos\theta \quad [53]$$

where D_{hkl} is the crystallite size (here determined from the (220), (311), (400) and (440) planes), 0.89 is the shape factor assuming spherical particles, θ is the Bragg's angle, β is the full-width at half-maximum (FWHM) of the experimental peaks and λ the X-ray wavelength (1.5418 Å). Nanoparticles have been found in all cases. The largest particle size is obtained in the sample of CoFe_2O_4 in good agreement with the described of Ahmed et al. [54].

XRD data of the samples obtained by the two preparation routes were analyzed by the Rietveld method using the FULLPROF program [46, 47]. The corresponding XRD profiles were refined considering an inverse spinel-type structure with a half of Fe^{3+} cations occupying the 8b positions with tetrahedral coordination, iron and cobalt atoms were placed randomly distributed in the 16c sites with octahedral coordination and O atoms in the 32e positions. In all cases, a good agreement between the observed and calculated profiles can be appreciated. As an example, Figure 2 shows the observed, calculated and difference profiles of powder diffraction data for the CP- Fe_3O_4 sample. A good agreement between the observed and calculated profiles can be appreciated. The refined crystallographic parameters of all samples investigated are given in Table 2.

A more pronounced reduction of a lattice parameter is observed for CP- Fe_3O_4 sample when the refinement is carried out considering only the presence of the magnetite phase, while this parameter approaches the theoretical value in the refinement that considers the presence of the magnetite and a small percentage of maghemite phases. These results indicate a partially oxidation of these sample which it does not happen with the rest of the synthesized samples [55]. The $d_{\text{M-O}}(t_d)$ (and $d_{\text{M-O}}(o_h)$) distances are in agreement with those calculated by using the corresponding Shannon radii values [52],

($\text{Co}^{2+}/\text{Fe}^{2+}$) atoms are centred in their respective distorted octahedra while (Fe^{3+}) atoms show four-fold coordination.

3.2. IR spectroscopy

Figure 3 shows the FTIR spectra of pure SiO_2 , $\text{CP-Fe}_3\text{O}_4@\text{SiO}_2$ and $\text{CP-Fe}_3\text{O}_4@\text{SiO}_2\text{-APTES}$ samples. Analogous FTIR spectra are observed in the samples $\text{CP-CoFe}_2\text{O}_4$, $\text{HT-Fe}_3\text{O}_4$ and $\text{HT-CoFe}_2\text{O}_4$ and their nanocomposites.

In all mentioned spectra can be distinguished two contributions. The first contribution shows absorption bands around 600 and 400 cm^{-1} . The maxima of the 400 cm^{-1} signal can't be clearly assigned due to the measurements condition. Nevertheless, it is observed a variation on the higher wavenumber band: 599 (FTIR spectrum of $\text{CP-Fe}_3\text{O}_4@\text{SiO}_2$ sample), 606 ($\text{HT-Fe}_3\text{O}_4@\text{SiO}_2$ sample), 590 and cm^{-1} ($\text{CP-CoFe}_2\text{O}_4@\text{SiO}_2$ sample) and 590 cm^{-1} ($\text{HT-CoFe}_2\text{O}_4@\text{SiO}_2$ sample). These two characteristic bands of an inverse spinel ferrite structure [56], correspond to intrinsic stretching vibrations of the M-O located at tetrahedral site (600 cm^{-1}) and octahedral site (400 cm^{-1}). It is well known that the frequency value at which the bands appear in the FTIR spectra depends on the cationic mass, the cation-oxygen bond force and the distance, so the frequency at which the bands absorption appear increases gradually as the metal-oxygen distance decreases and these results are in good agreement with those determined from the XRD data [57]. The second contribution contemplates the bands of silica. The broadband between 1099 and 1250 cm^{-1} were assigned to the modes of asymmetric vibration of O-Si-O and Si-O-Si bonds [58, 59], the 950, 800 and 470 cm^{-1} bands can be attributed to the presence of silanol (Si-OH) groups free surface, the symmetrical O-Si-O tension and the bending Si-O, respectively [60, 61]. The presence of all these bands show the association between magnetic cores and silica covering. The

registered spectra do not allow to visualize the presence of bands corresponding to the N-H bonds characteristic of the agent used for functionalization.

3.3. *Ninhydrin assays*

In order to confirm the functionalization of silica nanocomposites surfaces with amino groups, the reaction of synthesized materials with ninhydrin was performed [62].

Nanocomposite suspensions were treated with a 0.2% w/v solution of ninhydrin. After a 10 minute treatment in an ultrasonic bath, the samples were heated for 15 minutes in a water bath at approximately 80 ° C. After cooling, the nanocomposites were separated using an Nd magnet. In all cases, a purple supernatant was obtained, as shown in Figure 4. This color is obtained by the reaction of the ninhydrin with the amino groups, giving positive in the test and therefore, confirming the superficial functionalization of silica.

3.4. *TEM studies*

TEM images of Fe_3O_4 samples and their nanocomposites are shown in Figure 5.

Spherical particles can be observed for both CP- Fe_3O_4 (Figure 5a) and HT- Fe_3O_4 (Figure 5c), with a mean size 11.8 and 7.9 nm respectively, in good agreement with those calculated from XRD experiments. The magnetic dipole-dipole interaction at long-range existing between the particles can be the cause of the particle agglomerates shown in Figure 5c [63], probably originated in the drying process when preparing the sample to obtain images by TEM. A complete and homogeneous silica coating in the environment of aggregates of nanoparticles can be observed in Figures 5b (10 nm) and 5d (15 nm), of a greater thickness in the HT- Fe_3O_4 @ SiO_2 -APTES sample (Figure 5d). These results indicate that the increase in the thickness of the coating is favored in the smaller

particles obtained by hydrothermal. Similar results have been previously described by Ding et al. [64] for magnetite nanoparticles with different sizes and by Bassam el al. with respect to other magnetite-silica-TEOS structures, [65].

Figure 6 shows TEM images of cobalt synthesized samples. In this case, nanoparticles aggregates of 13.5 and 12.5 nm can be observed for CoFe_2O_4 cores obtained by coprecipitation (Figure 6a) and by hydrothermal synthesis (Figure 6c), respectively which are in good agreement with XRD results. These aggregates are covered with a layer of uniform and similar thickness, justifiable by the practically equivalent size nanoparticles constituted of synthesized magnetic cores (thickness of 14 and 15 nm for CP- $\text{CoFe}_2\text{O}_4@ \text{SiO}_2\text{-APTES}$ and HT- $\text{CoFe}_2\text{O}_4@ \text{SiO}_2\text{-APTES}$ respectively), in good agreement with described by Wang et al [66].

3.5. Magnetic studies

The magnetic field dependence of magnetization at room temperature of all synthesized magnetic nanocomposites is presented in Figures 7 and 8. Table 3 summarizes the magnetic parameters determinates from these graphics. A different magnetic behaviour is found for iron and cobalt materials. Fe_3O_4 samples show a practically superparamagnetic behaviour with very low coercive fields and M_r/M_s ratios (11-14 Oe and 0.02-0.03 respectively, see Table 3), regardless of the synthesis method used in the preparation of magnetic cores. By contrast, CoFe_2O_4 samples are ferromagnetic, being found greater values of the coercive fields and M_r/M_s ratios in samples of magnetic cores prepared by hydrothermal synthesis (between 748-879 Oe and 0.22-0.35). In general, the different behaviour of iron and cobalt samples can be explained by considering the different values of the magnetocrystalline anisotropy constants: $-1.2 \cdot 10^5$ erg/cm³ (samples of Fe_3O_4) and $1.8 \cdot 10^6$ erg/cm³ (samples of CoFe_2O_4), which leads a

higher value of coercive field of cobalt samples and, thus, a greater remnant [67]. As shown in Table 3, the M_r value determined in the iron samples vary between 0.64 and 1.99 emu/g, whereas in the cobalt samples this range is much higher (between 5.73-15.88 emu/g). This later result is in good agreement with Safi et al. [68] and can be explained by a partial loss of the spherical morphology of the particles.

As can be observed in Table 3, all CP- Fe_3O_4 samples present a reduction of the saturation magnetization values (M_s) respect to the theoretical value of bulk magnetite (92 emu/g) [69]. The value of CP- Fe_3O_4 core agrees with what we previously described [55]. A reduction of M_s is evidenced with the silica covering (32 emu/g) which is increased by functionalizing the silica with APTES (27 emu/g), justifiable considering the non-magnetic behaviour of the silica and APTES. The saturation magnetization of HT- Fe_3O_4 sample is somewhat smaller, which can be explained because the reduction in particle size generates surface effects where the magnetic moments are canted, losing directionally [70]. However, the reduction of saturation magnetization caused by coating and functionalization is like that achieved in the magnetic sample prepared by coprecipitation.

In the same way, CoFe_2O_4 samples present a reduction of the saturation magnetization values (M_s) respect to the theoretical value (50.1 emu/g) [67] and this reduction is smaller for the HT- CoFe_2O_4 sample. These results can be explained considering the spin canting present in particles and the difference found, due to the lower crystallinity of CP- CoFe_2O_4 sample, as it was found in XRD experiments. However, regardless of the synthesis method, when CoFe_2O_4 cores are cover or functionalized, regardless of the synthesis method, these reductions are more similar.

3.6. Adsorption assays

Chemistry adsorption assays of cations Cu^{2+} in aqueous solutions with contact time were carried out using all the synthesized nanocomposites at a maximum absorbance value of 635 nm. As an example, Figure 9 shows the curve obtained in the study for CP- Fe_3O_4 @ SiO_2 -APTES sample.

A decrease in absorbance is observed over time evidencing the absorption of copper in solution by the magnetic nanocomposite. After a rapid decrease in short times, this drop is softened due to the saturation of the functional groups ($-\text{NH}_2$) present on the surface of the coating, which marks the maximum value of copper that the sample is capable of retain by formation of the corresponding copper coordination compound. Table 4 summarizes the obtained results for each nanocomposite.

As reflected in the Table 4, all the investigated samples behave as adsorbent membranes of the Cu^{2+} cations, being, therefore, useful for the withdrawal of these cations in aqueous solution. These nanocomposites have an absorption capacity of more than 100 mg of Cu per g of sample, which is more than 10% of their own weight. The amount of Cu^{2+} removed from the solution presents a relationship with the average radius of the nanoparticles (calculated based on both core and shell dimensions of nanocomposites).

In the study carried out it is confirmed the greater capacity of adsorption of CP- Fe_3O_4 @ SiO_2 -APTES sample (161 mg Cu/g). This sample shows the lowest average radii (31.8 nm), resulting in a high greater surface area/volume ratio and greater availability of amino groups on the surface [71] which can allow the interaction with Cu^{2+} ions present in aqueous medium and the subsequent formation of bonds with these metal ions. This effect is also observed for the CP- CoFe_2O_4 @ SiO_2 -APTES nanocomposite, but in this case, a greater value of average radii (37.9 nm) leads to a lower capacity of adsorption of Cu^{2+} ions (142 mg Cu/g). This result can be justified by

considering the larger average size (13.5 nm) of the CP-CoFe₂O₄ magnetic cores that provides a smaller specific surface.

With regard to samples of nanocomposites whose cores were prepared by hydrothermal synthesis, the lower adsorption capacity is found in the HT-CoFe₂O₄@SiO₂-APTES sample, value close to that determined for HT-Fe₃O₄@SiO₂-APTES sample. Both samples show average sizes of 42.5 nm and 37.9 nm, respectively which indicates that a high value of the coating thickness reduces the adsorption capacity. These results are probably due, as Gilbert et al. [72] has pointed out and as seen here in the Figures 4d and 5d, to a high rate of powder aggregation. Also in this case, it is shown that the lower value of the surface area/volume ratio for HT-CoFe₂O₄@SiO₂-APTES sample leads to a lower adsorption capacity (110.1 mg Cu/g). with respect to determinate for HT-Fe₃O₄@SiO₂-APTES sample (120.6 mg Cu/g).

Different articles have described adsorption assays of cations of aqueous solutions adsorption values on coated Fe₃O₄ samples (pectin coated iron oxide -48.99 mg/g- [71], amine-functionalized silica magnetite -10.41mg/g- [73], amine functionalized Fe₃O₄ - 25.77 mg/g- [74], EDTA functionalized Fe₃O₄ -46.27 mg/g- [75], composite using waste fungal mycelium and Fe₃O₄-71.36 mg/g- [76], aminated polyacrylonitrile fibers - 31 mg/g- [77], among others. It is noted that the values obtained in this work are higher and like described for Fe₃O₄ chitosan beads samples 129 mg/g [78], although a higher absorption capacity is found here in the CP-Fe₃O₄@SiO₂-APTES sample.

4. Conclusion

In this study, amino-functionalized MFe₂O₄@SiO₂-APTES nanocomposites with a core-shell structure has been prepared by coprecipitation and hydrothermal synthesis to apply them in Cu²⁺ cations removal in aqueous media. XRD profiles shows that all

synthesized compounds crystallize in an inverse spinel structure. FTIR spectra evidence the presence of silica and the ninhydrin assays, its functionalization with APTES. The formation of the core-shell architecture is confirmed by TEM, where can be distinguished a uniform silica-cover around the particles. A higher shell thickness is found for the magnetic cores prepared by synthesis hydrothermal constituted by small nanoparticles. Nanocomposites maintains the magnetic behavior of their respective cores, superparamagnetism for Fe_3O_4 samples and ferrimagnetism for CoFe_2O_4 samples. A reduction of saturation magnetization is denoted when the nanoparticle is cover by non-magnetic silica. UV assays evidence a reduction of the copper concentration when saturating the amino groups present on the surface of the coatings that allows their removal from the solution aqueous. The maximum adsorption values ($161.7 \text{ g Cu}^{2+}/\text{mg}$), corresponding to the sample $\text{CP-Fe}_3\text{O}_4@\text{SiO}_2\text{-APTES}$, improves the results of the most of the magnetic copper sorbents, suggesting their future uses for environmental applications.

Acknowledgements

Fundación Neurociencias y Envejecimiento has supported this work through project 359/2014 as well as MINECO through the project MAT2016-80182-R. The authors thank the ICTS National Center for Electron Microscopy of the UCM for access.

References

- [1] S. Chowdhurya, M.A. J. Mazumder O. Al-Attasa, T. Husain, Heavy metals in drinking water: Occurrences, implications, and future needs in developing countries, *Sci. Total. Environ.* 569–570 (2016) 476-488.

- [2] M. Noreen, M. Shahid, M. Iqbal, J. Nisar, Measurement of cytotoxicity and heavy metal load in drains water receiving textile effluents and drinking water in vicinity of drains, *Measurement* 109 (2017) 88-99.
- [3] Q. Wu, H. Zhou, N. F. Tam, Y. Tian, Y. Tan, S. Zhou, Q. Li, Y. Chen, J. Y. S. Leung, Contamination, toxicity and speciation of heavy metals in an industrialized urban river: Implications for the dispersal of heavy metals, *Mar. Pollut. Bull.* 104 (2016) 153-161.
- [4] T.-K. L. Bui, L. C. Do-Hong, T.-S. Dao, T. C. Hoang, Copper toxicity and the influence of water quality of Dongnai River and Mekong River waters on copper bioavailability and toxicity to three tropical species, *Chemosphere* 144 (2016) 872-878.
- [5] A. Arulkumar, S. Paramasivam, R. Rajaram, Toxic heavy metals in commercially important food fishes collected from Palk Bay, Southeastern India, *Mar. Pollut. Bull.* 119 (2017) 454-459.
- [6] N. Aranda, R. M. Valls, M. Romeu, V. Sánchez-Martos, R. Albaladejo, S. Fernández-Castillejo, R. Nogués, Ú. Catalán, A. Pedret, A. Espinel, M. A. Delgado, V. Arija, R. Sola, M. Giralt, Consumption of seafood and its estimated heavy metals are associated with lipid profile and oxidative lipid damage on healthy adults from a Spanish Mediterranean area: A cross-sectional study, *Environ. Res.* 156 (2017) 644-651.
- [7] S. Guan, T. Palermo, J. Meliker, Seafood intake and blood cadmium in a cohort of adult avid seafood consumers, *Int. J. Hyg. Envir. Heal.* 218 (2015) 147-152.

- [8] M. E. Mahmoud, A. M.G. Nassar, S. A. Abou, A. Shimaa, M.T. Elweshahy, Factors optimization of super-fast removal of heavy metals from aqueous solution using microwave-enforced sorption on the surface of a novel nano-composite, *Sep. Purif. Technol.* 174 (2017) 493-501.
- [9] Z. Xia, L. Baird, N. Zimmerman, M. Yeager, Heavy metal ion removal by thiol functionalized aluminum oxide hydroxide nanowhiskers, *Appl. Surf. Sci.* 416 (2017) 565-573.
- [10] F. Bigdeli, H. Ghasempour, A. Azhdari, T.Ali Morsali, H. Hosseini-Monfared, Ultrasound-assisted synthesis of nano-structured Zinc (II)-based metal-organic frameworks as precursors for the synthesis of ZnO nano-structures, *Ultrason. Sonochem.* 37 (2017) 29-36.
- [11] T. J. Ainscough, P. Alagappan, D. L.Oatley-Radcliffe, Andrew R.Barron, A hybrid super hydrophilic ceramic membrane and carbon nanotube adsorption process for clean water production and heavy metal removal and recovery in remote locations, *J. Water Process Eng.* 19 (2017) 220-230.
- [12] J. Azamat, A. Khataee, Improving the performance of heavy metal separation from water using MoS₂ membrane: Molecular dynamics simulation, *Comp. Mat. Sci.* 137 (2017) 201-207.
- [13] W. Yao, J. Wang, P. Wang, X. Wang, S. Yu, Y. Zou, J. Hou, T. Hayat, A. Alsaedi, X. Wang, Synergistic coagulation of GO and secondary adsorption of heavy metal ions on Ca/Al layered double hydroxides, *Environ. Pollut.* 229 (2017) 827-836.

- [14] G. J. Rincon, E. J. La Motta, Simultaneous removal of oil and grease, and heavy metals from artificial bilge water using electro-coagulation/flotation, *J. Environ. Manage.* 144 (2014) 42-50.
- [15] P.O. Boamah, Y. Huang, M. Hua, Q. Zhang, J. Wu, J. Onumah, L.K. Sam-Amoah, Sorption of heavy metal ions onto carboxylate chitosan derivatives-A mini-review, *Ecotoxicol. Environ. Saf.* 116 (2015) 113–120.
- [16] Y.-L. Li, J. Wang, Z.-B. Yue, W. Tao, H.-B. Yang, Y.-F. Zhou, T.-H. Chen, Simultaneous chemical oxygen demand removal, methane production and heavy metal precipitation in the biological treatment of landfill leachate using acid mine drainage as sulfate resource, *J. Biosci. Bioeng.* 124 (2017) 71-75.
- [17] M. Taseidifar, F. Makavipour, R. M. Pashley, A.F.M. M. Rahman, Removal of heavy metal ions from water using ion flotation, *Environ. Technol.* 8 (2017) 182-190.
- [18] I. Petrinic, J. Korenak, D. Povodnik, C. Hélix-Nielsen, A feasibility study of ultrafiltration/reverse osmosis (UF/RO)-based wastewater treatment and reuse in the metalfinishing industry, *J. Clean. Prod.* 101 (2015) 1–9.
- [19] Y. Li, Z. Xu, S. Liu, J. Zhang, X. Yang, Molecular simulation of reverse osmosis for heavy metal ions using functionalized nanoporous graphenes, *Comp. Mater. Sci.* 139 (2017) 65–74.
- [20] D. Kołodynska, J. Krukowska-Bak, J. Kazmierczak-Razna, R. Pietrzak, Uptake of heavy metal ions from aqueous solutions by sorbents obtained from the spent ion exchange resins, *Micropor. Mesopor. Mat.* 244 (2017) 127-136.

- [21] M. Nemati, S.M. Hosseini, M. Shabanian, Novel electrodialysis cation exchange membrane prepared by 2-acrylamido-2-methylpropane sulfonic acid; heavy metal ions removal, *J. Hazard. Mater.* 337 (2017) 90–104.
- [22] S. M. Sorouraddin, M. A. Farajzadeh, T. Okhravi, Cyclohexylamine as extraction solvent and chelating agent in extraction and preconcentration of some heavy metals in aqueous samples based on heat-induced homogeneous liquid-liquid extraction, *Talanta* 175 (2017) 359–365.
- [23] A. Habibiyan, M. Ezoddin, N. Lamei, K. Abdi, M. Amini, M. Ghazi-khansari, Ultrasonic assisted switchable solvent based on liquid phase microextraction combined with micro sample injection flame atomic absorption spectrometry for determination of some heavy metals in water, urine and tea infusion samples, *J. Mol. Liq.* 242 (2017) 492–496.
- [24] H. Demey, T. Vincent, E. Guibal, A Novel Algal-Based Sorbent for Heavy Metal Removal, *Chem. Eng. J.* 332 (2018) 582-595
- [25] W. Peng, H. Li, Y. Liu, S. Song, A review on heavy metal ions adsorption from water by graphene oxide and its composites, *J. Mol. Liq.* 230 (2017) 496-504.
- [26] E. Da'na, Adsorption of heavy metals on functionalized-mesoporous silica: A review, *Micropor. Mesopor. Mat.* 247 (2017) 145-157.
- [27] M. Sajid, M. K. Nazal, Ihsanullah, N. Baig, A. M. Osman, Removal of heavy metals and organic pollutants from water using dendritic polymers based adsorbents: A critical review, *Sep. Purif. Technol.* 191 (2018) 400-423.

- [28] Ihsanullah, A. Abbas, A. M. Al-Amer, T. Laoui, M. A. Atieh, Heavy metal removal from aqueous solution by advanced carbon nanotubes: Critical review of adsorption applications, *Sep. Purif. Technol.* 157 (2016) 141-161.
- [29] M. K. Uddin, A review on the adsorption of heavy metals by clay minerals, with special focus on the past decade, *Chem. Eng. J.* 308 (15) (2017) 438-462
- [30] E. T. Tenório-Neto, A. Baraket, D. Kabbaj, N. Zine, A. Errachid, H. Fessi, M. H. Kunita, A. Elaissari. "Submicron magnetic core conducting polypyrrole polymer shell: Preparation and characterization". *Mater. Sci. Eng. C* 61 (2016) 688-694.
- [31] F. Yang, H. Chen, D. Liu, P. Xiong, W. Li, X. Chen, The microstructure and magnetic properties of FeCo@SiO₂ core-shell nanoparticles synthesized by using a solution method, *J. Alloy. Compd.* 728 (2017) 1153-1156.
- [32] N. Wang, L. Zhou, J. Guo, Q. Ye, J.-M. Lin, J. Yuan, Adsorption of environmental pollutants using magnetic hybrid nanoparticles modified with β -cyclodextrin, *Appl. Surf. Sci.* 305 (2014) 267-273.
- [33] M. Akkari, P. Aranda, A. Mayoral, M. García-Hernández, A. Ben Haj Amara, E. Ruiz-Hitzky, Sepiolite nanoplatform for the simultaneous assembly of magnetite and zinc oxide nanoparticles as photocatalyst for improving removal of organic pollutants, *J. Hazard. Mater.* 340 (2017) 281-290.
- [34] R. K. Gautam, M. C. Chattopadhyaya, Functionalized Magnetic Nanoparticles: Adsorbents and Applications, *Nanomaterials for Wastewater Remediation*. Amsterdam: Butterworth-Heinemann, Elsevier (2016) 139-159.

- [35] F. Oveisi, M. Nikazar, M. H. Razzaghi, M. Al-Sadat Mirrahimi, M. T. Jafarzadeh, Effective removal of mercury from aqueous solution using thiol-functionalized magnetic nanoparticles, *Environ. Nanotechnol. Monitoring Manage.* 7 (2017) 130-138.
- [36] L. I. Abd Ali, W. A. W. Ibrahim, A. Sulaiman, M. A. Kamboha, M. M. Sanagi, New chrysin-functionalized silica-core shell magnetic nanoparticles for the magnetic solid phase extraction of copper ions from water samples, *Talanta* 148 (2016) 191–199.
- [37] A. Asthana, R. Verma, A. K. Singh, Md. A. B. H. Susan, Glycine functionalized magnetic nanoparticle entrapped calcium alginate beads: A promising adsorbent for removal of Cu (II) ions, *J. Environ. Chem. Eng.* 4 (2016) 1985-1995.
- [38] S. Bao, K. Li, P. Ning, J. Peng, X. Jin, L. Tang, Highly effective removal of mercury and lead ions from wastewater by mercaptoamine-functionalised silica-coated magnetic nano-adsorbents: Behaviours and mechanisms, *Appl. Surf. Sci.* 393 (2017) 457-466.
- [39] S.P. Mun, Z. Cai, J. Zhang, Magnetic separation of carbon-encapsulated Fe nanoparticles from thermally-treated wood char, *Mater Lett*, 96 (2013) 5-7.
- [40] F. Zeb, W. Sarwer, K. Nadeem, M. Kamran, M. Mumtaz, H. Krenn, I. Letofsky-Papst, Surface spin-glass in cobalt ferrite nanoparticles dispersed in silica matrix, *J. Magn. Magn. Mater.* 407 (2016) 241–246.
- [41] S. Rohilla, S. Kumar, P. Aghamkar, S. Sunder, A. Agarwal, Investigations on structural and magnetic properties of cobalt ferrite/silica nanocomposites prepared by the coprecipitation method, *J. Magn. Magn. Mater.* 323 (2011) 897–902.

- [42] M. Amiri, M. Salavati-Niasari, A. Akbari, T. Gholami, Removal of malachite green (a toxic dye) from water by cobalt ferrite silica magnetic nanocomposite: Herbal and green sol-gel autocombustion synthesis, *Int. J. Hydrogen Energ.* 42 (2017) 24846-24860.
- [43] V.V. Korolev, A.G. Ramazanova, Adsorption of surfactants on superfine magnetite, A.V. Blinov, *Russ. Chem. Bull.* 51 (2002) 2044.
- [44] W. Jiang, Y. Wu, B. He, X. Zeng, K. Lai, Z. Gu, Effect of sodium oleate as a buffer on the synthesis of superparamagnetic magnetite colloids, *J. Colloid Interf. Sci.* 347 (2010) 1–7.
- [45] Y.-H. Deng, C.-C. Wang, J.-H. Hu, W.-L. Yang, S.-K. Fu, Investigation of formation of silica-coated magnetite nanoparticles via sol–gel approach, *Colloid. Surface. A* 262 (2005) 87–93.
- [46] J. Rodríguez-Carvajal, FULLPROF: A program for Rietveld refinement and pattern matching analysis, en Abstract of the Satellite Meeting of the XVth Congress of the International Union of Crystallography, Toulouse, France, (Universite' Paul Sabatier, Toulouse), (1990).
- [47] T. Roisnel, J. Rodriguez-Carvajal, WinPLOTR, plotr@llb.saclay.cea.fr, <http://www-llb.cea.fr/fullweb/winplotr/winplotr.htm>
- [48] Jasonov, P. G., D. K. Nougaliyev, B. V Burov, F. Heller, A modernized coercivity spectrometer, *Geol. Carpathica* 49 (1998) 224–225.

- [49] P. S. Yoo, B. W. Lee, C. Liu, Effects of pH Value, Reaction Time, and Filling Pressure on the Hydrothermal Synthesis of ZnFe_2O_4 Nanoparticles, *IEEE T. Magn.* 51 (2015) 2003004.
- [50] M. E. Fleet, The Structure of Magnetite, *Acta Crystallogr. B.* 37 (1981) 917–920.
- [51] N. V. Proskurina, V. A. Cherepanov, O. S. Golynets, V. I. Voronin, Phase equilibria and structure of solid solutions in the La–Co–Fe–O system at 1100 °C, *Inorg. Mater.* 40 (2004) 955–959.
- [52] R.D. Shannon, Revised effective ionic radii and systematic studies of interatomic distances in halides and chalcogenides, *Acta Crystallogr. A* 32 (1976) 751–767.
- [53] P. Scherrer, Bestimmung der Größe und der inneren Struktur von Kolloidteilchen mittels Röntgenstrahlen, *Nachrichten von der Gesellschaft der Wissenschaften zu Göttingen, Mathematisch-Physikalische Klasse*, 26 (1918) 98–100.
- [54] A. Ahmed, N. Okasha, S.I. El-Dek, Influence of Co content on the characterization and magnetic properties of magnetite, *Ceram. Int.* 36 (2010) 1529–1533.
- [55] P. Arévalo, J. Isasi, A.C. Caballero, J.F. Marcoc, F. Martín-Hernández, Magnetic and structural studies of Fe_3O_4 nanoparticles synthesized via coprecipitation and dispersed in different surfactants, *Ceram. Int.* 43 (2017) 10333–10340.
- [56] M. Vadivel, R. R. Babu, M. Arivanandhan, K. Ramamurthi, Y. Hayakawa, Role of SDS surfactant concentrations on the structural, morphological, dielectric and magnetic properties of CoFe_2O_4 nanoparticles, *RSC Advances* 5 (2015) 27060–27068.

- [57] Y. Köseoglu, F. Alan, M. Tan, R. Yilgin, M. Özürk, “Low temperature hydrothermal synthesis and characterization of Mn doped cobalt ferrite nanoparticles” *Ceram. Int.* 38 (2012) 3625–3643.
- [58] L. Alcaraz, J. Isasi, Synthesis and study of $Y_{0.9}Ln_{0.1}VO_4$ nanophosphors and $Y_{0.9}Ln_{0.1}VO_4@SiO_2$ luminescent nanocomposites with $Ln=Eu, Dy, Er$, *Ceram. Int.*, 43 (2017) 5311-5318.
- [59] Q. Chang, L. Zhu, C. Yu, H. Tang, Synthesis and properties of magnetic and luminescent $Fe_3O_4/SiO_2/Dye/SiO_2$ nanoparticles, *J. Lumin* 128 (2008) 1890–1895.
- [60] A.M Donia, A.A Atia, W.A Al-amrani, A.M El-Nahas, Effect of structural properties of acid dyes on their adsorption behaviour from aqueous solutions by amine modified silica, *J Hazard Mater.* 161 (2009) 1544–1550.
- [61] D. C. Culita, C. M. Simonescu, R. E. Patescu, M. Dragne, N. Stanica, O. Oprea, o-Vanillin functionalized mesoporous silica-coated magnetitenanoparticles for efficient removal of Pb(II) from water, *J. Solid State Chem.* 238 (2016) 311–320.
- [62] B. Chertok, A. E. David, V. C. Yang, Polyethylene imine-modified iron oxide nanoparticles for brain tumour drug delivery using magnetic targeting and intra-carotid administration, *Biomaterials* 31 (2010) 6317-6324.
- [63] D. Eberbeck, F. Wiekhorst, U. Steinhoff, L. Trahms, Aggregation behaviour of magnetic nanoparticle suspensions investigated by magnetorelaxometry, *J. Phys.: Condens. Matter* 18 (2006) S2829–S2846.
- [64] H. L. Ding, Y. X. Zhang, S. Wang, J. M. Xu, S. C. Xu, G. H. Li, $Fe_3O_4@SiO_2$ Core/Shell Nanoparticles: The Silica Coating Regulations with a Single

Core for Different Core Sizes and Shell Thicknesses, *Chem. Mater.* 24 (2012) 4572–4580.

[65] B. Saif, C. Wang, D. Chuan, S. Shuang, Synthesis and Characterization of Fe_3O_4 Coated on APTES as Carriers for Morin-Anticancer Drug, *J. Biomater. Nanobiotechnol.*, 2015, 6, 267-275.

[66] H. Wang, J. Huang, L. Ding, D. Li, Y. Han, A facile synthesis of monodisperse $\text{CoFe}_2\text{O}_4/\text{SiO}_2$ nanoparticles, *Appl. Surf. Sci.* 257 (2011) 7107–7112.

[67] V. Pillai, D.O. Shah, Synthesis of high-coercivity cobalt ferrite particles using water-in-oil microemulsions, *J. Magn. Magn. Mater.* 163 (1996) 243–248.

[68] R. Safi, A. Ghasemi, R. Shoja-Razavi, E. Ghasemi, T. Sodaee, Rietveld structure refinement, cations distribution and magnetic features of CoFe_2O_4 nanoparticles synthesized by co-precipitation, hydrothermal, and combustion methods, *Ceram. Int.* 42 (2016) 6375–6382.

[69] E. Petrovský, E. Herrero-Bervera, T. Harinarayana, D. Ivers, *The Earth's Magnetic Interior*, Springer Science & Business Media, 2011.

[70] S. Mørup, E. Brok, C. Frandsen, Spin Structures in Magnetic Nanoparticles, *J. Nanomater.* 2013 (2013), 720629.

[71] J.-L. Gong, X.-Y. Wang, G.-M. Zeng, L. Chen, J.-H. Deng, X.-R. Zhang, Q.-Y. Niu, Copper(II) removal by pectin–iron oxide magnetic nanocomposite adsorbent, *Chem. Eng. J.* (2012) 100–107.

- [72] B. Gilbert, R. K. Ono, K. A. Ching, C. S. Kim, The effects of nanoparticle aggregation processes on aggregate structure and metal uptake, *J. Colloid Interf. Sci.* 339 (2009) 285–295
- [73] Y. Lin, H. Chen, K. Lin, B. Chen, C. Chiou, Application of magnetic particles modified with amino groups to adsorb copper ions in aqueous solution, *J. Environ. Sci.* (2011) 44–50.
- [74] H.Y. Mei, C. Man, H.Z. Bo, Effective removal of Cu(II) ions from aqueous solution by amino-functionalized magnetic nanoparticles, *J. Hazard. Mater.* (2010) 392–399.
- [75] Y. Liu, M. Chen, Y. Hao, Study on the adsorption of Cu(II) by EDTA functionalized Fe₃O₄ magnetic nanoparticles, *Chem. Eng. J.* (2013) 46–54.
- [76] Y. Ren, M. Zhang, D. Zhao, Synthesis and properties of magnetic Cu(II) ion imprinted composite adsorbent for selective removal of copper, *Desalination* (2008) 135–149.
- [77] S. Deng, R. Bai, J. P. Chen, Aminated Polyacrylonitrile Fibers for Lead and Copper Removal, *Langmuir* 2003,19, 5058-5064.
- [78] W. Jiang, W. Wang, B. Pan, Q. Zhang, W. Zhang, L. Lv, Facile Fabrication of Magnetic Chitosan Beads of Fast Kinetics and High Capacity for Copper Removal, *ACS Appl. Mater. Interfaces* 2014, 6, 3421–3426.

Figure captions

Figure 1. XRD patterns of the synthesized samples: (a) CP-Fe₃O₄, (b) HT-Fe₃O₄, (c) CP-CoFe₂O₄ and (d) HT-CoFe₂O₄.

Figure 2. Observed (red line), calculated (black line) and difference (blue line) XRD patterns of CP-Fe₃O₄ samples.

Figure 3. FTIR spectra of pure SiO₂, CP-Fe₃O₄@SiO₂ and CP-Fe₃O₄@SiO₂-APTES samples.

Figure 4. Ninhydrin test for HT-CoFe₂O₄@SiO₂- APTES sample.

Figure 5. CP-Fe₃O₄ (a), CP-Fe₃O₄@SiO₂-APTES (b), HT-Fe₃O₄ (c) and HT-Fe₃O₄@SiO₂- APTES (d).

Figure 6. CP-CoFe₂O₄ (a), CP-CoFe₂O₄@SiO₂-APTES (b), HT- CoFe₂O₄ (c) and HT-CoFe₂O₄@SiO₂-APTES (d).

Figure 7. Magnetic field dependence of the magnetization of the magnetic cores (black), samples covered by silica (red) and magnetic silica-APTES nanocomposites (blue) for: CP-Fe₃O₄ (a), HT-Fe₃O₄ (b).

Figure 8. Magnetic field dependence of the magnetization of the magnetic cores (black), samples covered by silica (red) and magnetic silica-APTES nanocomposites (blue) for: CP-CoFe₂O₄ (a), HT- CoFe₂O₄ (b).

Figure 9. Adsorption Cu²⁺ cations curve over time of CP-Fe₃O₄@SiO₂-APTES sample.

Table 1. Lattice parameters and average crystallite size.

Sample	a (Å)	d _{hkl} (nm)
CP-Fe ₃ O ₄	8.383(3)	11
HT-Fe ₃ O ₄	8.398(3)	7
Fe ₃ O ₄ [50]	8.3941	—
CP-CoFe ₂ O ₄	8.379(4)	13
HT-CoFe ₂ O ₄	8.387(4)	12
CoFe ₂ O ₄ [51]	8.3860	—

Table 2. Crystallographic parameters obtained in the refinements of MFe_2O_4 samples.

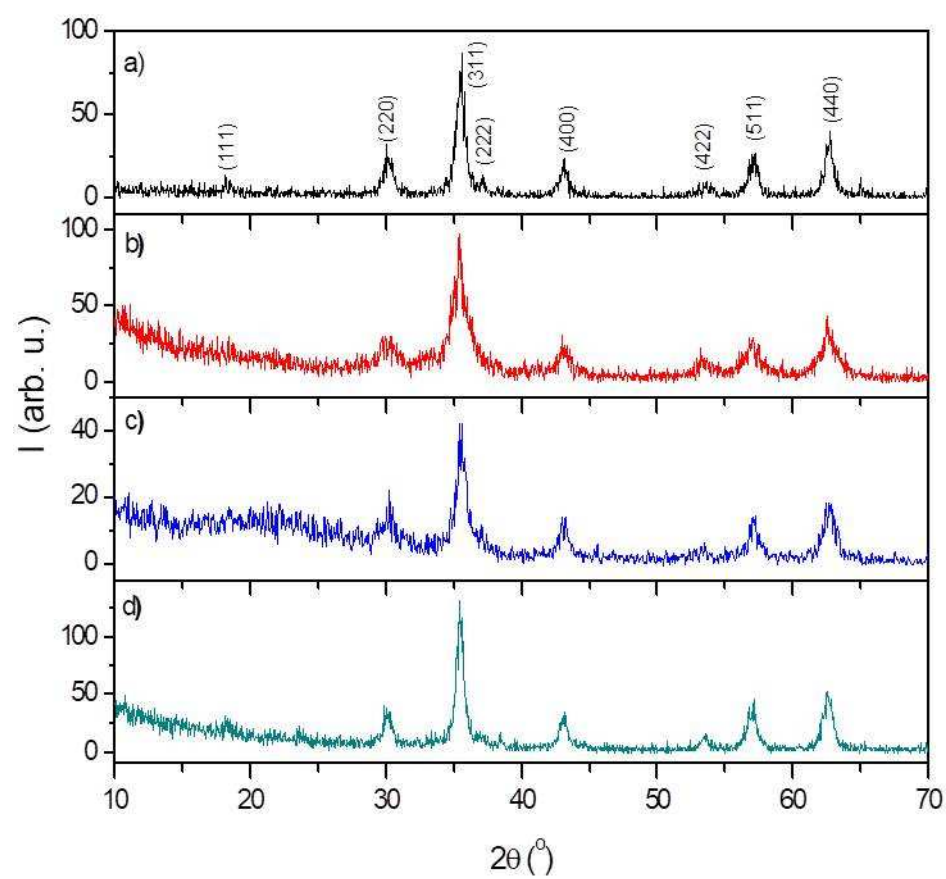
[illegible]

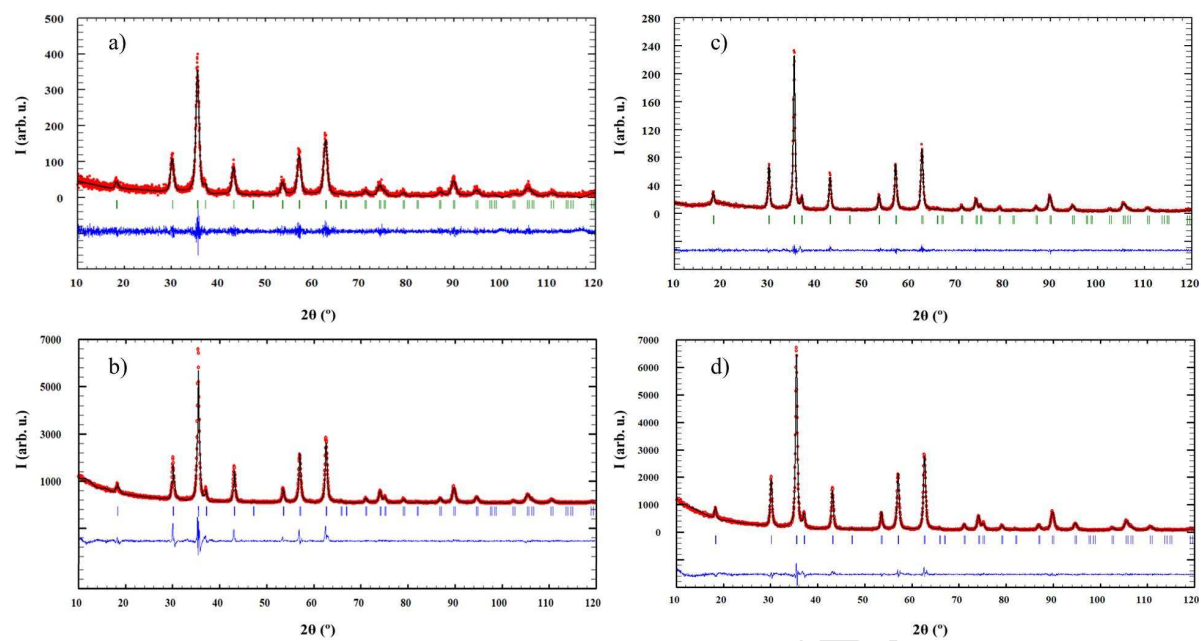
Table 3. Magnetic parameters obtained from the M vs H loops.

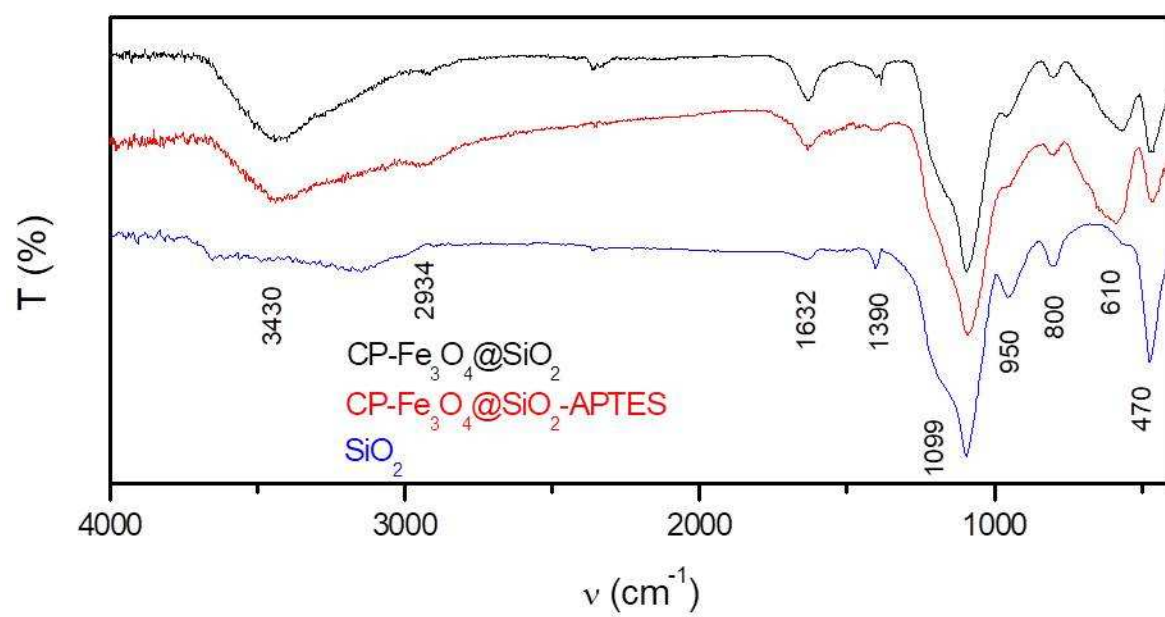
Sample	H _c (Oe)	M _s (emu/g)	M _r (emu/g)	M _r /M _s
CP-Fe ₃ O ₄	14	67.48	1.99	0.03
CP-Fe ₃ O ₄ @SiO ₂	11	32.72	0.77	0.02
CP-Fe ₃ O ₄ @SiO ₂ -APTES	11	27.65	0.79	0.03
HT-Fe ₃ O ₄	12	41.44	1.03	0.02
HT-Fe ₃ O ₄ @SiO ₂	12	36.59	0.81	0.02
HT-Fe ₃ O ₄ @SiO ₂ - APTES	13	28.36	0.64	0.02
CP-CoFe ₂ O ₄	400	39.96	8.74	0.22
CP-CoFe ₂ O ₄ @SiO ₂	651	32.22	9.90	0.31
CP-CoFe ₂ O ₄ @SiO ₂ -APTES	556	25.48	5.73	0.22
HT-CoFe ₂ O ₄	748	50.11	15.88	0.32
HT-CoFe ₂ O ₄ @SiO ₂	842	25.49	8.72	0.34
HT-CoFe ₂ O ₄ @SiO ₂ - APTES	879	23.80	8.35	0.35

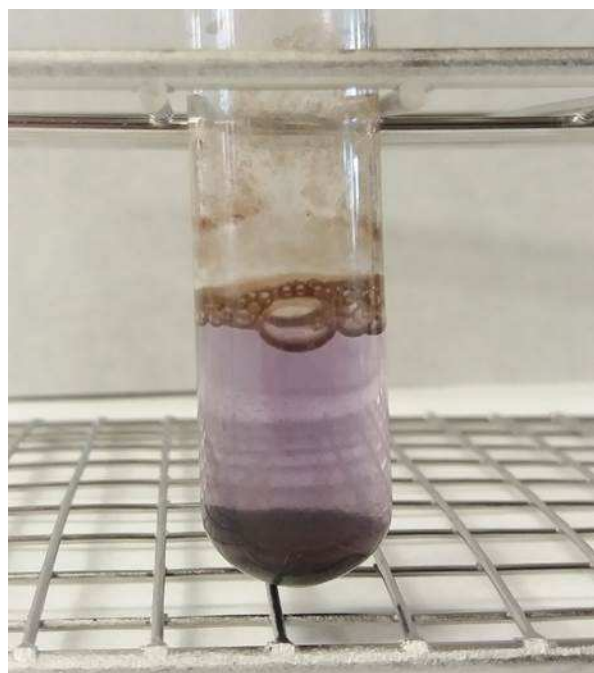
Table 4. Parameters of copper adsorption by APTES-functionalized nanocomposites.

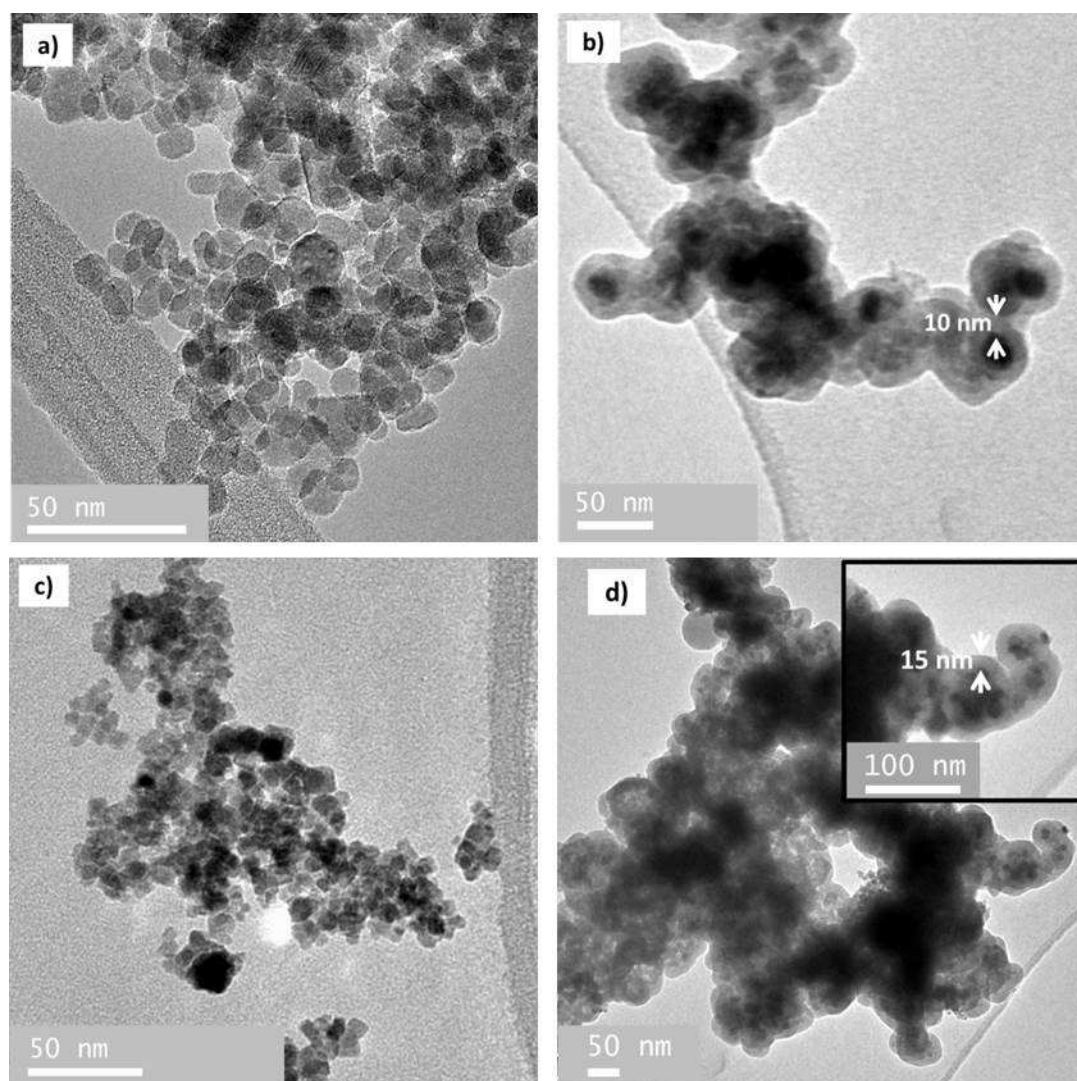
Sample	$\Delta(\text{Abs})$	$\Delta[\text{Cu}^{2+}]$ (mM)	mg Cu/g	SiO ₂ -APTES thickness (nm)
CP-Fe ₃ O ₄ @SiO ₂ -APTES	0.204	2.54	161.7	10
HT-Fe ₃ O ₄ @SiO ₂ - APTES	0.156	1.90	120.6	15
CP-CoFe ₂ O ₄ @SiO ₂ -APTES	0.182	2.25	142.8	14
HT-CoFe ₂ O ₄ @SiO ₂ - APTES	0.144	1.73	110.1	15

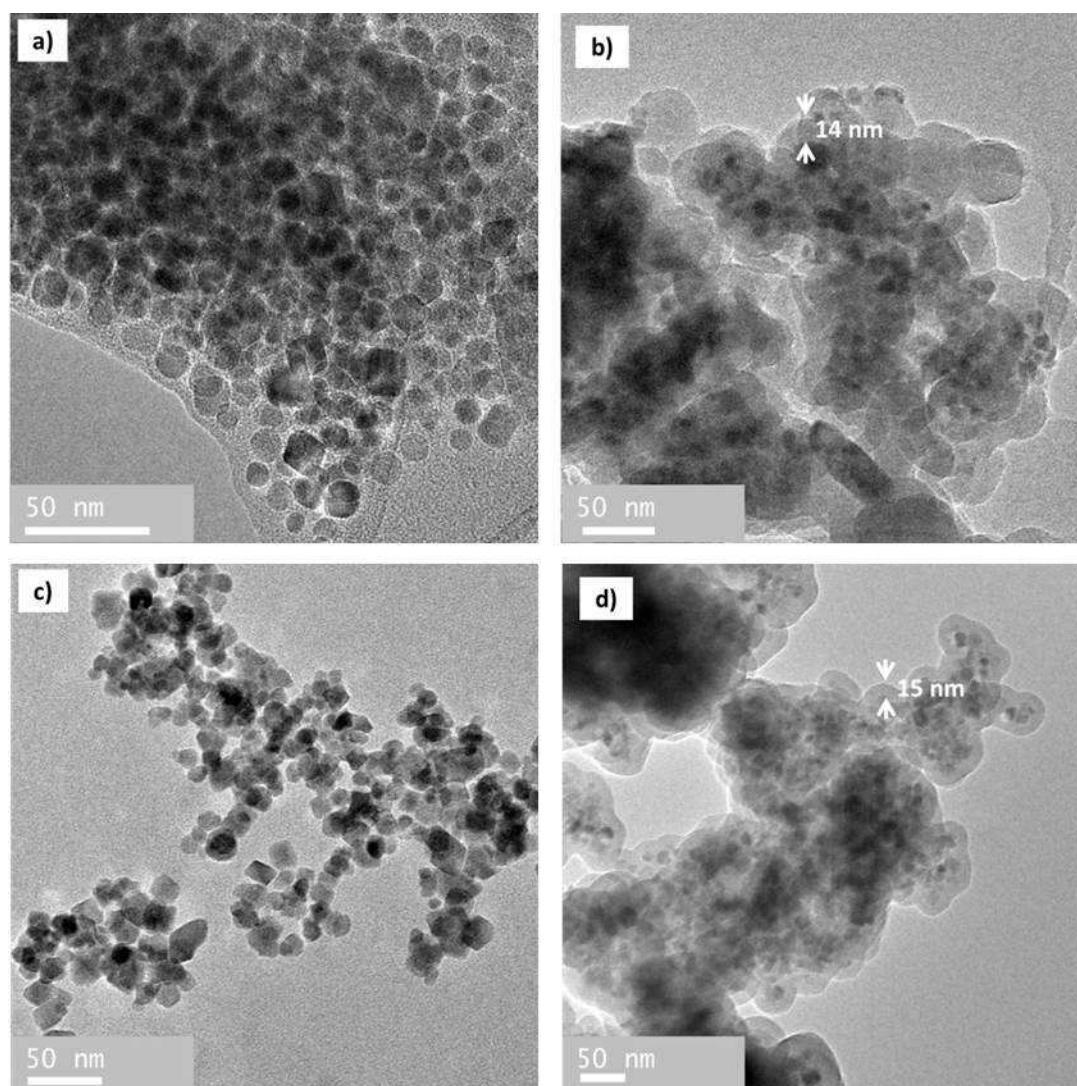


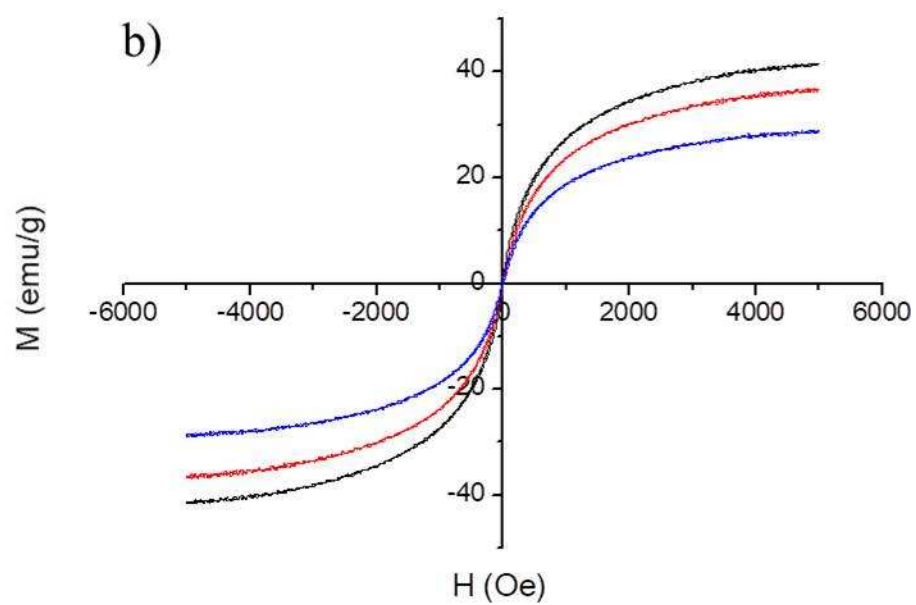
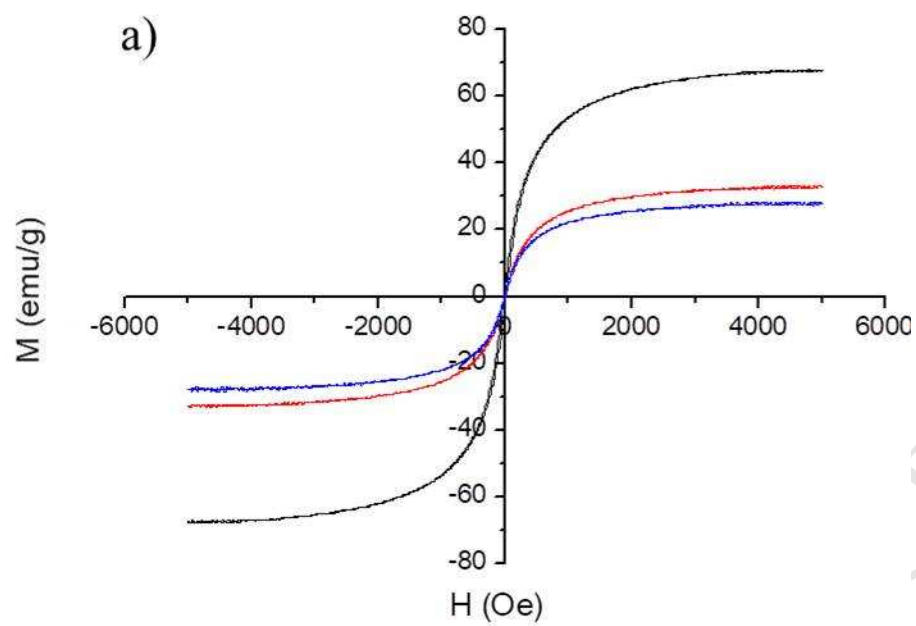


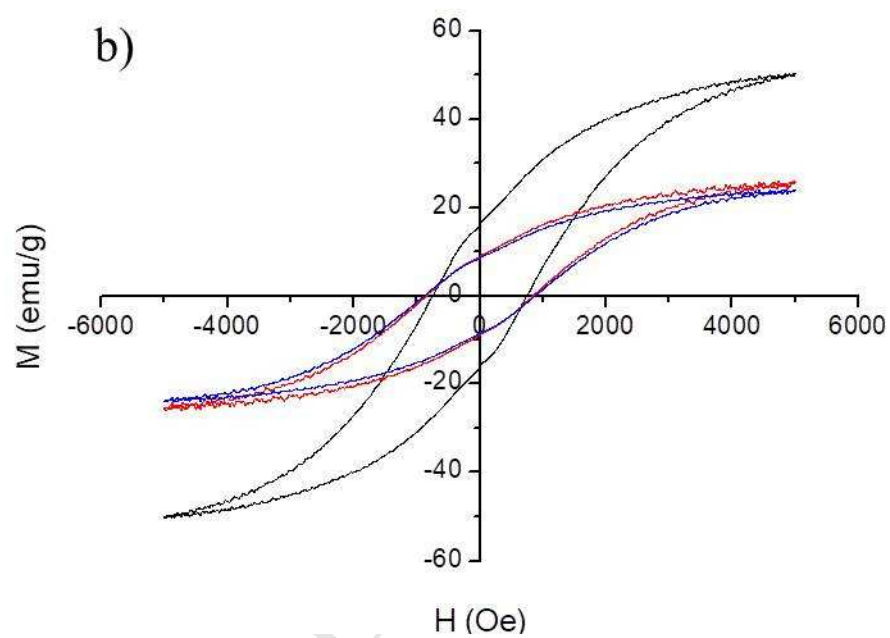
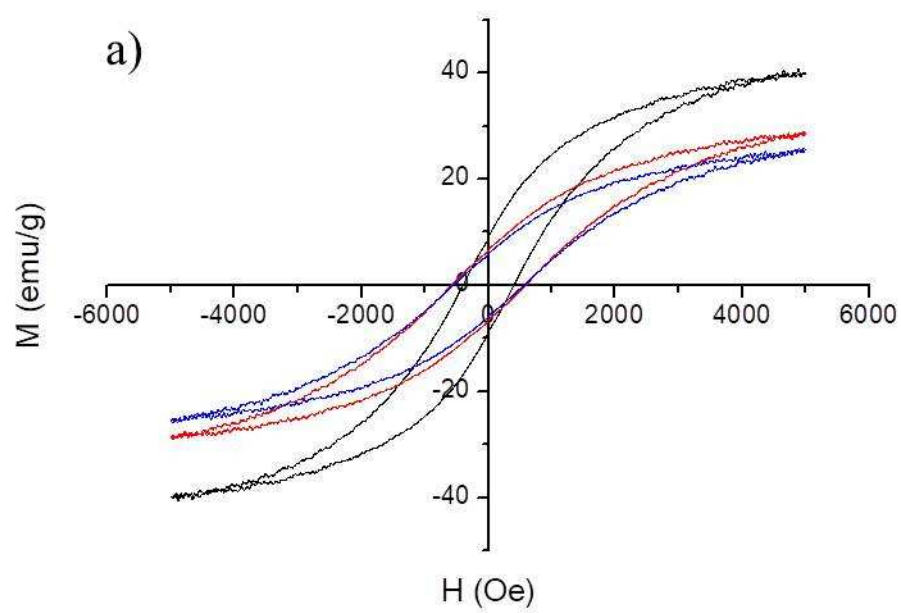


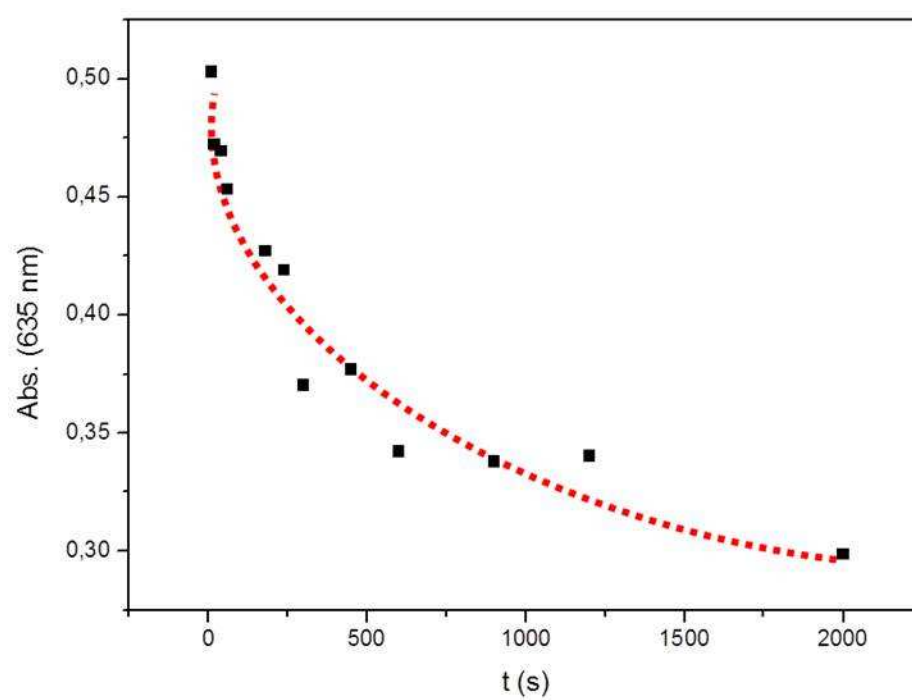












Highlights

- $\text{MFe}_2\text{O}_4@\text{SiO}_2\text{-NH}_2$ nanocomposites are prepared from different magnetic cores.
- A uniform silica coating around all magnetic nanoparticles is confirmed by TEM.
- Cu^{2+} removal assays evidence ion capture by the amino groups on composite surfaces.
- All composites reach an adsorption capacity of more than 10% of their own weight.
- The maximum adsorption values improve those found in most magnetic sorbents.